Inorg. Chem. **2005**, *44*, 9353–9359

New Metal Iodates: Syntheses, Structures, and Characterizations of Noncentrosymmetric $La(IO_3)_3$ and $NaYI_4O_{12}$ and Centrosymmetric β-$Cs_2I_4O_{11}$ and $Rb_2I_6O_{15}(OH)_2 \cdot H_2O$

Kang Min Ok and P. Shiv Halasyamani*

Department of Chemistry and Center for Materials Chemistry, 136 Fleming Building, University of Houston, Houston, Texas 77204-5003

Received August 5, 2005

Four new metal iodates, β-$Cs_2I_4O_{11}$, $Rb_2I_6O_{15}(OH)_2 \cdot H_2O$, $La(IO_3)_3$, and $NaYI_4O_{12}$, have been synthesized hydrothermally, and the structures were determined by single-crystal X-ray diffraction techniques. All of the reported materials contain I^{5+} cations that are in asymmetric coordination environments attributable to their stereoactive lone pair. Second-order nonlinear optical measurements on noncentrosymmetric $La(IO_3)_3$ and $NaYI_4O_{12}$, using 1064-nm radiation, indicate that both materials have second-harmonic-generating properties with efficiencies of approximately 400 $\times$ SiO_2. Converse piezoelectric measurements revealed d_{33} values of 5 and 138 pm V^{-1} for $La(IO_3)_3$ and $NaYI_4O_{12}$, respectively. Infrared and Raman spectroscopy and thermogravimetric analyses are also presented for all of the reported materials. Crystal data: β-$Cs_2I_4O_{11}$, monoclinic, space group $P2_1/n$ (No. 14), with $a = 12.7662(14)$ Å, $b = 7.4598(8)$ Å, $c = 14.4044(16)$ Å, $\beta = 106.993(2)°$, $V = 1311.9(2)$ Å^3, and $Z = 4$; $Rb_2I_6O_{15}(OH)_2 \cdot H_2O$, triclinic, space group $P\bar{1}$ (No. 2), with $a = 7.0652(17)$ Å, $b = 7.5066(18)$ Å, $c = 18.262(4)$ Å, $\alpha = 79.679(4)°$, $\beta = 85.185(4)°$, $\gamma = 70.684(4)°$, $V = 898.9(4)$ Å^3, and $Z = 2$; $La(IO_3)_3$, monoclinic, space group Cc (No. 9), with $a = 12.526(2)$ Å, $b = 7.0939(9)$ Å, $c = 27.823(4)$ Å, $\beta = 101.975(4)°$, $V = 2418.4(6)$ Å^3, and $Z = 4$; $NaYI_4O_{12}$, monoclinic, space group Cc (No. 9), with $a = 31.235(3)$ Å, $b = 5.5679(5)$ Å, $c = 12.5451(12)$ Å, $\beta = 91.120(3)°$, $V = 2181.3(4)$ Å^3, and $Z = 4$.

Introduction

Oxide materials containing cations in asymmetric coordination environments are of current interest owing to their technologically important properties such as second-harmonic generation (SHG), piezoelectricity, ferroelectricity, and pyroelectricity.[1−4] In addition to having asymmetrically coordinated cations, materials exhibiting these properties must also be crystallographically noncentrosymmetric (NCS). A number of strategies have been suggested to increase the incidence of acentricity in any new material.[5−10] We have focused on utilizing cations that are asymmetric coordination environments attributable to second-order Jahn−Teller distortions.[11−15] Specifically, we have synthesized new acentric materials that contain d^0 transition metals (Ti^{4+}, Nb^{5+}, W^{6+}, etc.) and/or cations with lone pairs (Se^{4+}, Te^{4+}, I^{5+}, etc.). Not only do these materials exhibit second-order nonlinear optical behavior, i.e., SHG or frequency doubling, but some of the materials are also ferroelectric.[16] It should

* To whom correspondence should be addressed. E-mail: psh@uh.edu. Phone: 713-743-3278. Fax: 713-743-0796.

(1) Jona, F.; Shirane, G. *Ferroelectric Crystals*; Pergamon Press: Oxford, U.K., 1962.
(2) Cady, W. G. *Piezoelectricity; an Introduction to the Theory and Applications of Electromechanical Phenomena in Crystals*; Dover: New York, 1964.
(3) Lang, S. B. *Sourcebook of Pyroelectricity*; Gordon & Breach Science: London, 1974.
(4) Galy, J.; Meunier, G. *J. Solid State Chem.* **1975**, *13*, 142.
(5) Bruce, D.; Wilkinson, A. P.; While, M. G.; Bertrand, J. A. *J. Solid State Chem.* **1996**, *125*, 228.
(6) Kepert, C. J.; Prior, T. J.; Rosseinsky, M. J. *J. Am. Chem. Soc.* **2000**, *122*, 5158.
(7) Maggard, P. A.; Stern, C. L.; Poeppelmeier, K. R. *J. Am. Chem. Soc.* **2001**, *123*, 7742.
(8) Welk, M. E.; Norquist, A. J.; Arnold, F. P.; Stern, C. L.; Poeppelmeier, K. R. *Inorg. Chem.* **2002**, *41*, 5119.
(9) Evans, O. R.; Lin, W. *Acc. Chem. Res.* **2002**, *35*, 511.
(10) Hwu, S.-J.; Ulutagay-Kartin, M.; Clayhold, J. A.; Mackay, R.; Wardojo, T. A.; O'Connor, C. J.; Kraweic, M. *J. Am. Chem. Soc.* **2002**, *124*, 12404.
(11) Bader, R. F. W. *Mol. Phys.* **1960**, *3*, 137.
(12) Bader, R. F. W. *Can. J. Chem.* **1962**, *40*, 1164.
(13) Pearson, R. G. *J. Am. Chem. Soc.* **1969**, *91*, 4947.
(14) Pearson, R. G. *J. Mol. Struct.: THEOCHEM* **1983**, *103*, 25.
(15) Wheeler, R. A.; Whangbo, M.-H.; Hughbanks, T.; Hoffmann, R.; Burdett, J. K.; Albright, T. A. *J. Am. Chem. Soc.* **1986**, *108*, 2222.

10.1021/ic051340u CCC: $30.25
Published on Web 11/01/2005

Table 1. Crystallographic Data for β-$Cs_2I_4O_{11}$, $Rb_2I_6O_{15}(OH)_2{\cdot}H_2O$, $La(IO_3)_3$, and $NaYI_4O_{12}$

formula	β-$Cs_2I_4O_{11}$	$Rb_2I_6O_{15}(OH)_2{\cdot}H_2O$	$La(IO_3)_3$	$NaYI_4O_{12}$
fw	949.42	1224.38	1990.83	1623.00
space group	$P2_1/n$ (No. 14)	$P\bar{1}$ (No. 2)	Cc (No. 9)	Cc (No. 9)
a (Å)	12.7662(14)	7.0652(17)	12.526(2)	31.235(3)
b (Å)	7.4598(8)	7.5066(18)	7.0939(9)	5.5679(5)
c (Å)	14.4044(16)	18.262(4)	27.823(4)	12.5451(12)
α (deg)	90	79.679(4)	90	90
β (deg)	106.993(2)	85.185(4)	101.975(4)	91.120(3)
γ (deg)	90	70.684(4)	90	90
V (Å^3)	1311.9(2)	898.9(4)	2418.4(6)	2181.3(4)
Z	4	2	4	4
T (°C)	293.0(2)	293.0(2)	293.0(2)	293.0(2)
λ (Å)	0.71073	0.71073	0.71073	0.71073
ρ_{calcd} (g cm^{-3})	4.807	4.509	5.468	4.942
μ (mm^{-1})	15.013	15.833	16.812	16.77
$R(F)^a$	0.0293	0.0493	0.0333	0.0527
$R_w(F_o^2)^b$	0.0728	0.1362	0.0861	0.1424

^{a} $R(F) = \sum||F_o| - |F_c||/\sum|F_o|$. ^{b} $R_w(F_o^2) = [\sum w(F_o^2 - F_c^2)^2/\sum w(F_o^2)^2]^{1/2}$.

be noted that the symmetry requirements for ferroelectricity are more restrictive compared with SHG because the former must be not only acentric but also polar. In this paper, we expand our acentric characterization techniques to include converse piezoelectric measurements. Although the phenomena are completely different, piezoelectricity and second-order nonlinear optical behavior are described mathematically by the same tensor, d_{ijk}.[17] In this paper, we report on the synthesis and structure of four new iodates, β-$Cs_2I_4O_{11}$, $Rb_2I_6O_{15}(OH)_2{\cdot}H_2O$, $La(IO_3)_3$, and $NaYI_4O_{12}$. The latter two are NCS and have been characterized by SHG and converse piezoelectric measurements.

Experimental Section

Reagents. Cs_2CO_3 (Aldrich, 99+%), RbOH (Aldrich, 99%), Na_2CO_3 (Alfa Aesar, 99.5%), La_2O_3 (Aldrich, 99.9%), Y_2O_3 (Aldrich, 99.99+%), and HIO_3 (Aldrich, 99.5+%) were used as received.

Syntheses. For β-$Cs_2I_4O_{11}$, 0.652 g (2.00×10^{-3} mol) of Cs_2CO_3 and 5.000 g (2.84×10^{-2} mol) of HIO_3 were combined with 5 mL of H_2O. For $Rb_2I_6O_{15}(OH)_2{\cdot}H_2O$, 10 mL of a 0.85 M RbOH solution and 5.000 g (2.84×10^{-2} mol) of HIO_3 were combined. For $La(IO_3)_3$, 0.326 g (1.00×10^{-3} mol) of La_2O_3 and 5.000 g (2.84×10^{-2} mol) of HIO_3 were combined with 10 mL of H_2O. For $NaYI_4O_{12}$, 0.212 g (2.00×10^{-3} mol) of Na_2CO_3, 0.226 g (1.00×10^{-3} mol) of Y_2O_3, and 4.000 g (2.27×10^{-2} mol) of HIO_3 were combined with 10 mL of H_2O. Each solution was placed in a 23-mL Teflon-lined autoclave that was subsequently sealed. The autoclaves were gradually heated to 220 °C, held for 4 days, and cooled slowly to room temperature at a rate of 6 °C h^{-1}. The products were recovered by filtration and washed with water and ethanol. Pure colorless crystals, the only product from each reaction, of β-$Cs_2I_4O_{11}$, $Rb_2I_6O_{15}(OH)_2{\cdot}H_2O$, $La(IO_3)_3$, and $NaYI_4O_{12}$ were obtained in 91%, 62%, 83%, and 79% yields, respectively, based on the corresponding alkali carbonate or lanthanide oxide.

Single-Crystal X-ray Diffraction. For β-$Cs_2I_4O_{11}$, a colorless block ($0.16 \times 0.26 \times 0.28$ mm^3), for $Rb_2I_6O_{15}(OH)_2{\cdot}H_2O$, a colorless plate ($0.04 \times 0.16 \times 0.30$ mm^3), for $La(IO_3)_3$, a colorless rhomboid block ($0.10 \times 0.12 \times 0.14$ mm^3), and for $NaYI_4O_{12}$, a colorless plate ($0.02 \times 0.20 \times 0.22$ mm^3) were used for single-crystal data analyses. All of the data were collected using a Siemens SMART diffractometer equipped with a 1K CCD area detector using graphite monochromated Mo Kα radiation. A hemisphere of data was collected using a narrow-frame method with scan widths of 0.30° in ω and an exposure time of 25 s frame^{-1}. The first 50 frames were remeasured at the end of the data collection to monitor instrument and crystal stability. The maximum correction applied to the intensities was <1%. The data were integrated using the Siemens SAINT program,[18] with the intensities corrected for Lorentz, polarization, air absorption and absorption attributable to the variation in the path length through the detector faceplate. Ψ scans were used for the absorption correction on the hemisphere of data. The data were solved and refined using SHELXS-97 and SHELXL-97, respectively.[19,20] All of the metal atoms were refined with anisotropic thermal parameters and converged for $I > 2\sigma(I)$. All calculations were performed using the WinGX-98 crystallographic software package.[21] Relevant crystallographic data are listed in Table 1, and selected bond distances are given in Table 2.

Powder X-ray Diffraction. Powder X-ray diffraction was used to confirm the phase purity for each sample. The X-ray powder diffraction data were collected on a Scintag XDS2000 diffractometer at room temperature (Cu Kα radiation, $\theta-\theta$ mode, flat-plate geometry) equipped with a Peltier germanium solid-state detector in the 2θ range 5−60° with a step size of 0.02° and a step time of 1 s.

Infrared (IR) and Raman Spectroscopy. IR spectra were recorded on a Matteson FTIR 5000 spectrometer in the 400−4000-cm^{-1} range, with the sample pressed between two KBr pellets. Raman spectra were recorded at room temperature on a Digilab FTS 7000 spectrometer equipped with a germanium detector with the powder sample placed in separate capillary tubes. Excitation was provided by a Nd:YAG laser at a wavelength of 1064 nm, and the output laser power was 500 mW. The spectral resolution was ~4 cm^{-1}, and 100 scans were collected for each sample.

Thermogravimetric Analysis (TGA). TGA was carried out on a TGA 2950 thermogravimetric analyzer (TA instruments). The sample was contained within a platinum crucible and heated in air at a rate of 10 °C min^{-1} to 800 °C.

Second-Order Nonlinear Optical and Converse Piezoelectric Measurements. Powder SHG measurements on polycrystalline La-

(16) Chi, E. O.; Gandini, A.; Ok, K. M.; Zhang, L.; Halasyamani, P. S. *Chem. Mater.* **2004**, *16*, 3616.
(17) Nye, J. F. *Physical Properties of Crystals*; Oxford University Press: Oxford, U.K., 1957.
(18) *SAINT, Program for Area Detector Absorption Correction*, version 4.05; Siemens Analytical X-ray Instruments: Madison, WI, 1995.
(19) Sheldrick, G. M. *SHELXS-97—A program for automatic solution of crystal structures*; University of Göttingen: Göttingen, Germany, 1997.
(20) Sheldrick, G. M. *SHELXL-97—A program for crystal structure refinement*; University of Göttingen: Göttingen, Germany, 1997.
(21) Farrugia, L. J. *J. Appl. Crystallogr.* **1999**, *32*, 837.

Table 2. Selected Bond Distances (Å) for β-$Cs_2I_4O_{11}$, $Rb_2I_6O_{15}(OH)_2{\cdot}H_2O$, $La(IO_3)_3$, and $NaYI_4O_{12}$

β-$Cs_2I_4O_{11}$		$Rb_2I_6O_{15}(OH)_2{\cdot}H_2O$		$La(IO_3)_3$		$NaYI_4O_{12}$	
I(1)−O(1)	1.791(4)	I(1)−O(1)	2.323(8)	I(1)−O(1)	1.814(13)	I(1)−O(1)	1.818(16)
I(1)−O(2)	2.106(4)	I(1)−O(2)	1.802(8)	I(1)−O(2)	1.828(12)	I(1)−O(2)	1.829(16)
I(1)−O(3)	2.125(4)	I(1)−O(3)	1.800(9)	I(1)−O(3)	1.781(13)	I(1)−O(3)	2.452(16)
I(1)−O(4)	1.790(4)	I(1)−O(4)	1.923(9)	I(2)−O(4)	1.814(11)	I(1)−O(4)	1.839(17)
I(2)−O(3)	1.927(4)	I(2)−O(5)	1.796(8)	I(2)−O(5)	1.795(11)	I(2)−O(5)	1.820(15)
I(2)−O(3)	2.481(4)	I(2)−O(6)	1.869(8)	I(2)−O(6)	1.830(12)	I(2)−O(6)	1.811(16)
I(2)−O(6)	1.799(4)	I(2)−O(7)	2.428(8)	I(3)−O(7)	1.781(13)	I(2)−O(7)	1.797(15)
I(2)−O(7)	1.798(4)	I(2)−O(8)	1.815(8)	I(3)−O(8)	1.791(12)	I(2)−O(8)	2.420(16)
I(3)−O(2)	1.938(4)	I(3)−O(6)	2.102(8)	I(3)−O(9)	1.816(12)	I(3)−O(9)	1.830(16)
I(3)−O(2)	2.441(4)	I(3)−O(9)	1.762(8)	I(4)−O(10)	1.811(12)	I(3)−O(10)	1.811(16)
I(3)−O(9)	1.785(4)	I(3)−O(10)	2.211(8)	I(4)−O(11)	1.799(11)	I(3)−O(11)	1.788(15)
I(3)−O(10)	1.784(4)	I(3)−O(11)	1.795(8)	I(4)−O(12)	1.784(13)	I(4)−O(12)	1.838(16)
I(4)−O(5)	1.808(4)	I(4)−O(7)	1.804(8)	I(5)−O(13)	1.814(12)	I(4)−O(13)	1.803(14)
I(4)−O(8)	1.816(4)	I(4)−O(10)	1.862(8)	I(5)−O(14)	1.773(13)	I(4)−O(14)	1.802(17)
I(4)−O(11)	1.809(5)	I(4)−O(12)	1.788(8)	I(5)−O(15)	1.821(13)	I(5)−O(8)	1.827(14)
		I(5)−O(1)	1.828(8)	I(6)−O(16)	1.807(11)	I(5)−O(15)	1.805(16)
		I(5)−O(13)	1.813(8)	I(6)−O(17)	1.846(11)	I(5)−O(16)	1.800(14)
		I(5)−O(14)	1.796(9)	I(6)−O(18)	1.786(13)	I(6)−O(3)	1.811(14)
		I(6)−O(15)	1.900(8)	I(7)−O(19)	1.835(11)	I(6)−O(17)	1.841(17)
		I(6)−O(16)	1.793(8)	I(7)−O(20)	1.844(11)	I(6)−O(18)	1.836(16)
		I(6)−O(17)	1.793(8)	I(7)−O(21)	1.820(12)	I(7)−O(19)	1.798(17)
				I(8)−O(22)	1.810(11)	I(7)−O(20)	1.833(15)
				I(8)−O(23)	1.826(11)	I(7)−O(21)	1.827(17)
				I(8)−O(24)	1.801(11)	I(8)−O(22)	1.836(14)
				I(9)−O(25)	1.777(11)	I(8)−O(23)	1.839(14)
				I(9)−O(26)	1.831(11)	I(8)−O(24)	1.808(17)
				I(9)−O(27)	1.835(12)		

$(IO_3)_3$ and $NaYI_4O_{12}$ were performed on a modified Kurtz-NLO system[22] using 1064-nm radiation. A detailed description of the equipment and the methodology used has been published.[23,24] No index-matching fluid was used in any of the experiments. Powders with particle size 45−63 μm were used for comparing SHG intensities. Converse piezoelectric measurements were performed using a Radiant Technologies RT66A piezoelectric test system with a TREK (model 609E-6) high-voltage amplifier, Precision materials analyzer, Precision high-voltage interface, and MTI 2000 fotonic sensor. Polycrystalline $La(IO_3)_3$ and $NaYI_4O_{12}$ were pressed into 12-mm-diameter and ~0.8-mm-thick pellets. A conducting silver paste was applied to both sides of the pellet surfaces for electrodes. A maximum voltage of 700 V was applied to the samples.

Results and Discussion

Structures. β-$Cs_2I_4O_{11}$. β-$Cs_2I_4O_{11}$ has a pseudo-three-dimensional crystal structure consisting of asymmetric IO_3 and IO_4 groups separated by Cs^+ cations (see Figure 1). In connectivity terms, the structure may be written as $\{3[IO_{2/3}O_{2/1}]^{1/3-}[IO_{3/1}]^{1-}\}^{2-}$, with the charge balance maintained by the two Cs^+ cations. Three of the I^{5+} cations are linked to four O atoms in a "seesaw" environment with bond distances ranging from 1.784(4) to 2.481(4) Å. These bond distances are consistent with those of previously reported iodates.[25−29] The IO_4 groups form two-dimensional hexagonal tungsten oxide-like layers consisting of six-membered rings, with the IO_4 polyhedra alternating orientation as one proceeds around the ring such that the layers result in a centrosymmetric environment similar to that of α-$Cs_2I_4O_{11}$ (see Figures 1 and 2).[30] In addition, there are three very long I−O contacts

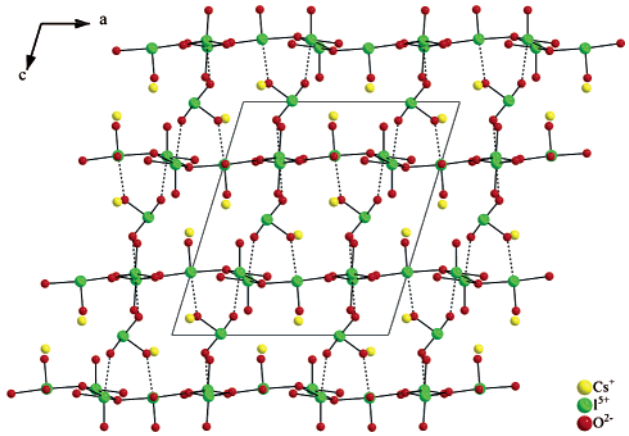

Figure 1. Ball-and-stick representation of β-$Cs_2I_4O_{11}$ in the *ac* plane. The dashed lines indicate long I−O interactions, giving the structure a pseudo-three-dimensional topology.

ranging from 2.583(5) to 2.644(5) Å, which have been drawn as dashed lines in Figure 1. These long contacts effectively link the IO_4 layers through the IO_3 group and give β-$Cs_2I_4O_{11}$ a pseudo-three-dimensional topology. The three-coordinate I^{5+} cations are in a distorted trigonal-pyramidal environment, with I−O bond distances ranging from 1.808(4) to 1.816(4) Å. The IO_3 groups, therefore, serve as *interlayer* linkers. Each Cs^+ is in a 9-fold coordination environment, with Cs−O contacts ranging from 3.145(5) to 3.544(5) Å. Bond-valence calculations[31,32] resulted in values of 0.83 for Cs^+ and 4.98−5.11 for I^{5+}.

(22) Kurtz, S. K.; Perry, T. T. *J. Appl. Phys.* **1968**, *39*, 3798.
(23) Ok, K. M.; Bhuvanesh, N. S. P.; Halasyamani, P. S. *J. Solid State Chem.* **2001**, *161*, 57.
(24) Porter, Y.; Ok, K. M.; Bhuvanesh, N. S. P.; Halasyamani, P. S. *Chem. Mater.* **2001**, *13*, 1910.
(25) Alcock, N. W. *Acta Crystallogr., Sect. B* **1972**, *28*, 2783.
(26) Coquet, E.; Crettez, J. M.; Pannetier, J.; Bouillot, J.; Damien, J. C. *Acta Crystallogr., Sect. B* **1983**, *39*, 408.
(27) Lucas, B. W. *Acta Crystallogr., Sect. C* **1984**, *40*, 1989.
(28) Svensson, C.; Stahl, K. *J. Solid State Chem.* **1988**, *77*, 112.
(29) Stahl, K.; Szafranski, M. *Acta Chem. Scand.* **1992**, *46*, 1146.
(30) Ok, K. M.; Halasyamani, P. S. *Angew. Chem., Int. Ed.* **2004**, *43*, 5489.
(31) Brown, I. D.; Altermatt, D. *Acta Crystallogr., Sect. B* **1985**, *41*, 244.

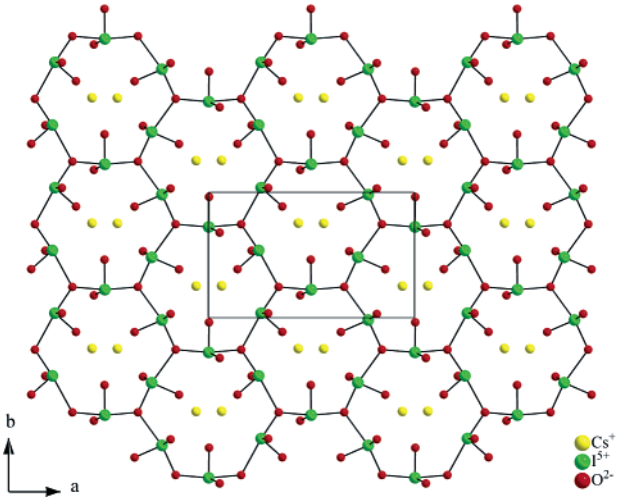

Figure 2. Ball-and-stick representation of β-$Cs_2I_4O_{11}$ in the *ab* plane, indicating one layer of the structure. Note how six-membered rings are formed by IO_4 polyhedra.

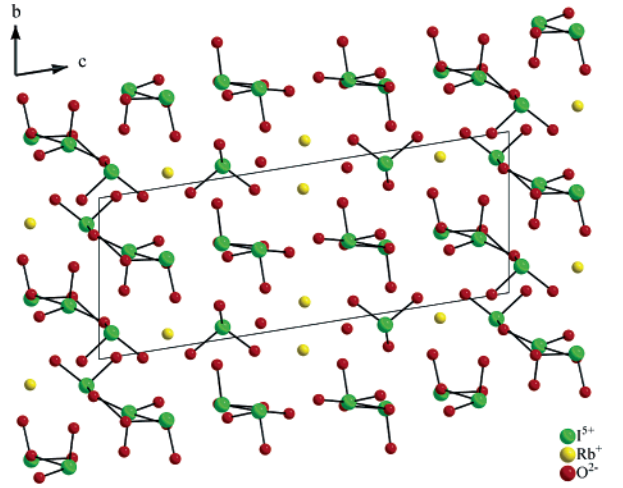

Figure 3. Ball-and-stick representation of $Rb_2I_6O_{15}(OH)_2{\cdot}H_2O$ in the *bc* plane. Note that the structure consists of the free $IO_2(OH)$ polyhedra, $[I_2O_5(OH)]^-$ dimers, iodate chains, Rb^+ cations, and H_2O molecules.

$Rb_2I_6O_{15}(OH)_2{\cdot}H_2O$. $Rb_2I_6O_{15}(OH)_2{\cdot}H_2O$ exhibits a one-dimensional crystal structure that consists of $IO_2(OH)$ polyhedra, $[I_2O_5(OH)]^-$ dimers, and IO_3 and IO_4 polyhedra. The IO_3 and IO_4 polyhedra form chains that run along the [100] direction (see Figures 3 and 4). The iodate chains are also separated by Rb^+ cations and H_2O molecules. With free $IO_2(OH)$ polyhedra and $[I_2O_5(OH)]^-$ dimers, the oxygen atoms, O(4) and O(15) from each group, are OH groups. To identify the positions of H^+, the hydrogen bonds in the structure were analyzed. We observe that strong hydrogen bonds occur from O(4) and O(15) to the terminal oxygen atoms of adjacent chains [O(4)···O(13) 2.592(4) Å; O(15)···O(8) 2.614(6) Å]. Moreover, bond-valence calculations on these terminal oxygen sites gave very similar values of 1.30 and 1.43 for O(4) and O(15), respectively, which are also consistent with our model. In addition, the IR spectrum confirms the presence of I−OH groups (see spectroscopic studies). Additionally, the terminal oxygen atom O(17) is also involved in hydrogen bonds with the water molecule [O(17)···O(w1) 2.808(6) Å]. In connectivity terms, the structure can be formulated as $\{2[IO_{2/2}O_{2/1}]^- [IO_{2/2}O_{1/1}]^+ [IO_{2/1}O_{1/2}]^0 [IO_{2/1}OH]^0 [IO_{2/1}O_{1/2}OH]^-\}^{2-}$, with the charge balance maintained by the two Rb^+ cations. The I^{5+} cations are linked to three and four oxygen atoms in a distorted trigonal-pyramidal and seesaw environment, respectively, with I−O bond distances ranging from 1.762(8) to 2.428(8) Å. Bond-valence calculations[31,32] resulted in values 1.08−1.15 and 4.85−5.17 for Rb^+ and I^{5+}, respectively.

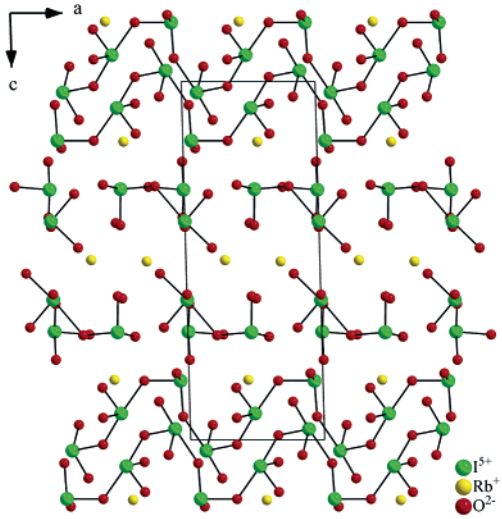

Figure 4. Ball-and-stick representation of $Rb_2I_6O_{15}(OH)_2{\cdot}H_2O$ in the *ac* plane. The iodate chains are running along the *a* axis, resulting in a one-dimensional structure.

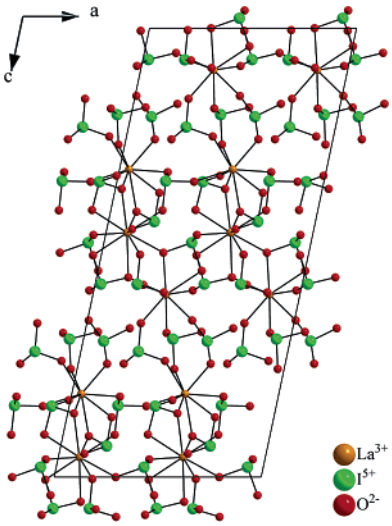

Figure 5. Ball-and-stick representation of $La(IO_3)_3$ in the *ac* plane. Note that the lanthanum trimers are inter- and intraconnected by asymmetric IO_3 polyhedra to form a three-dimensional crystal structure.

$La(IO_3)_3$. $La(IO_3)_3$ exhibits a three-dimensional crystal structure that consists of LaO_9 polyhedra that are connected by asymmetric IO_3 groups (see Figure 5). The three unique La^{3+} are bonded to nine oxygen atoms in a tricapped trigonal-prismatic environment, with bond distances ranging from 2.416(13) to 2.834(12) Å. The I^{5+} cations are linked to three oxygen atoms in a distorted trigonal-pyramidal environment, with I−O bond distances ranging from 1.773(13) to 1.846(11) Å. Structurally, $La(IO_3)_3$ is composed of edge-shared LaO_9 polyhedra along the [001] direction to form trimers.

(32) Brese, N. E.; O'Keeffe, M. *Acta Crystallogr., Sect. B* **1991**, *47*, 192.

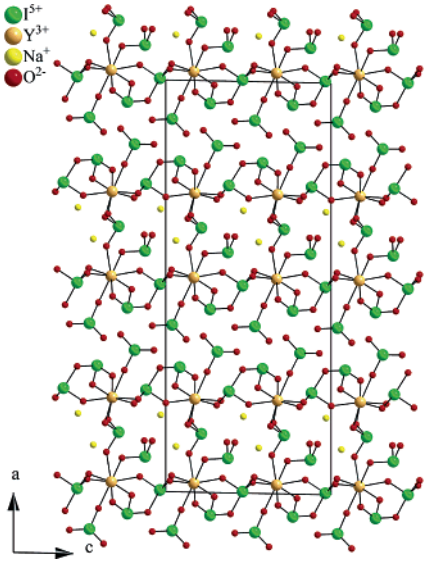

Figure 6. Ball-and-stick representation of $NaYI_4O_{12}$ in the *ac* plane. YO_8 polyhedra are linked by asymmetric IO_3 and IO_4 polyhedra to form a two-dimensional crystal structure. Note that a net moment is observed by IO_3 polyhedra pointing in the *c* direction, resulting in a NCS environment.

These lanthanum trimers are inter- and intraconnected by asymmetric IO_3 groups to form a three-dimensional framework structure (see Figure 5). In connectivity terms, the structure may be written as a neutral three-dimensional framework of $\{2[LaO_{7/2}O_{2/3}]^{5.333-}$ $[LaO_{6/2}O_{4/3}]^{5.667-}$ $3[IO_{2/2}O_{1/1}]^{+}$ $4[IO_{2/2}O_{1/3}]^{2.333+}$ $2[IO_{3/2}]^{2+}\}^{0}$. Bond-valence calculations[31,32] resulted in values of 3.08−3.21 for La^{3+} and 4.75−5.25 for I^{5+}.

$NaYI_4O_{12}$. $NaYI_4O_{12}$ exhibits a two-dimensional layered structure, with YO_8 polyhedra linked to asymmetric IO_3 and IO_4 polyhedra (see Figure 6). Each Y^{3+} cation is bonded to eight oxygen atoms in a square antiprismatic environment, with bond distances ranging from 2.274(14) to 2.587(16) Å. All of the eight oxygen atoms are further bonded to I^{5+} cations. The I^{5+} cations are linked to either three or four oxygen atoms, resulting in a highly distorted trigonal-pyramidal or seesaw environment owing to the nonbonded electron pair. The distances for the I−O bonds range from 1.788(15) to 2.452(16) Å. In connectivity terms, the structure may be written as $\{2[YO_{8/2}]^{5-}$ $3[IO_{2/1}O_{1/2}]^{0}$ $3[IO_{3/2}]^{2+}$ $2[IO_{4/2}]^{+}\}^{2-}$, with the charge balance retained by two Na^{+} cations. The connectivity of the yttrium and iodine polyhedra within each layer generates eight-membered-ring channels along the [010] direction (see Figure 6). Na^{+} cations reside in the channels. Bond-valence calculations[31,32] resulted in values of 0.99−1.02 for Na^{+}, 3.03−3.10 for Y^{3+}, and 4.82−5.39 for I^{5+}.

IR and Raman Spectroscopy. The IR and Raman spectra of β-$Cs_2I_4O_{11}$, $Rb_2I_6O_{15}(OH)_2{\cdot}H_2O$, $La(IO_3)_3$, and $NaYI_4O_{12}$ iodate compounds reveal I−O vibrations in the regions of ca. 600−840 and 310−540 cm^{-1}. With $Rb_2I_6O_{15}(OH)_2{\cdot}H_2O$, the broad stretches centered at 3446 and 1633 cm^{-1} can be assigned to stretching and bending modes of water molecules, respectively, and the vibrations at 3167 and 1162 cm^{-1} are attributed to the framework −OH groups. The IR and Raman vibrations and assignments are listed in Table 3. The assignments are consistent with those previously reported.[33−35]

Table 3. IR and Raman Vibrations (cm^{-1}) for β-$Cs_2I_4O_{11}$, $Rb_2I_6O_{15}(OH)_2{\cdot}H_2O$, $La(IO_3)_3$, and $NaYI_4O_{12}$

β-$Cs_2I_4O_{11}$		$Rb_2I_6O_{15}(OH)_2{\cdot}H_2O$				$La(IO_3)_3$		$NaYI_4O_{12}$	
ν_{I-O}	δ_{I-O}	ν_{I-O}	δ_{I-O}	ν_{O-H}	δ_{O-H}	ν_{I-O}	δ_{I-O}	ν_{I-O}	δ_{I-O}
IR (cm^{-1})									
831	502	819	526	3446	1633	835	518	840	520
818	450	808	501	3167	1162	823	501	821	503
801	431	773	455			802	458	798	476
781	423	757	435			777	449	765	457
767	412	738	416			761	437	740	445
742		721	408			738		719	420
693		671				721		701	
674		640				711		688	
		613				682		667	
		601				669		655	
						617		617	
								607	
Raman (cm^{-1})									
813	524	817	389			825	450	817	524
802	486	794	362			814	401	802	474
775	432	763	347			796	387	775	439
756	374	752	331			770		759	401
732		732	316			755		740	370
		717				746		721	
		636				725		709	
		613				711			
		601				683			
						634			

TGA. The thermal behavior of β-$Cs_2I_4O_{11}$, $Rb_2I_6O_{15}(OH)_2{\cdot}H_2O$, $La(IO_3)_3$, and $NaYI_4O_{12}$ was investigated using TGA. None of the materials reported in this paper is stable at higher temperatures. In each case, decompositions through thermal disproportionation occurred between 280 and 510 °C, indicating volatilization. For β-$Cs_2I_4O_{11}$, 1 equiv of I_2 and 3.5 equiv of O_2 are lost at approximately 400 °C. Calcd (exptl): 38.53% (38.52%). Another 1 equiv of I_2 is lost at around 550 °C, Calcd (exptl): 21.74% (21.19%). Finally, the remaining I_2, O_2, and Cs_2O begin to volatilize around 630 °C. $Rb_2I_6O_{15}(OH)_2{\cdot}H_2O$ revealed a weight loss of 4.06% between room temperature and ca. 190 °C, which is consistent with the loss of free water molecules and framework −OH groups. Calcd: 4.19%. A total of 2 mol of I_2 and 2 mol of O_2 are lost at approximately 380 °C. Calcd (exptl): 49.00% (47.63%). A total of 0.5 mol of I_2 and 1.5 mol of O_2 are subsequently lost at approximately 480 °C. Calcd (exptl): 29.30% (28.94%). The remainder of I_2, O_2, and Rb_2O volatilize completely around 660 °C. With $La(IO_3)_3$ (molecular formula: $La_3I_9O_{27}$), 1.5 equiv of I_2 is lost at approximately 280 °C. Calcd (exptl): 19.12% (19.16%). Above 280 °C, 3 equiv of I_2 and 11.25 mol of O_2 are lost at around 530 °C, leaving 1.5 mol of La_2O_3 at 800 °C. Calcd (exptl): 69.65% (69.98%). $NaYI_4O_{12}$ (molecular formula: $Na_2Y_2I_8O_{24}$) shows a weight loss at 410 °C that is attributed to the loss of 1.5 mol of I_2 and 1.5 mol of O_2. Calcd (exptl): 26.41% (26.24%). The remaining 2.5 mol of I_2, 9 equiv of O_2, and 1 mol of Na_2O begin to volatilize around 520 °C,

(33) Sykora, R. E.; Ok, K. M.; Halasyamani, P. S.; Wells, D. M.; Albrecht-Schmitt, T. E. *Chem. Mater.* **2002**, *14*, 2741.
(34) Sykora, R. E.; Ok, K. M.; Halasyamani, P. S.; Albrecht-Schmitt, T. E. *J. Am. Chem. Soc.* **2002**, *124*, 1951.
(35) Shehee, T. C.; Sykora, R. E.; Ok, K. M.; Halasyamani, P. S.; Albrecht-Schmitt, T. E. *Inorg. Chem.* **2003**, *42*, 457.

leaving 1 mol of Y_2O_3 at 800 °C. Calcd (exptl): 81.09% (82.93%). The TGA curves for all four materials have been deposited as Supporting Information.

Acentric Properties. SHG. Powder SHG measurements, using 1064-nm radiation, indicated that both $La(IO_3)_3$ and $NaYI_4O_{12}$ have SHG efficiencies of 400 × α-SiO_2. The SHG efficiencies are on the order of $BaTiO_3$ and are comparable to other NCS iodates such as HIO_3 (300 × α-SiO_2),[22] $LiIO_3$ (300 × α-SiO_2),[22] $NdMoO_2(IO_3)_4(OH)$ (350 × α-SiO_2),[35] $AMoO_3(IO_3)$ (A = Rb or Cs, 400 × α-SiO_2),[34] and α-$Cs_2I_4O_{11}$ (300 × α-SiO_2).[30] By sieving $La(IO_3)_3$ and $NaYI_4O_{12}$ into various particle sizes, ranging from 20 to 150 μm, and measuring the SHG as a function of the particle size, we were able to determine the type 1 phase-matching capabilities of the materials. We determined that $La(IO_3)_3$ is phase-matchable, whereas $NaYI_4O_{12}$ is not (see the Supporting Information). As previously shown, once the SHG efficiency has been measured and the phase-matching behavior determined, the average NLO susceptibility, $\langle d_{eff}\rangle_{exp}$, can be estimated.[36] $\langle d_{eff}\rangle_{exp}$ for $La(IO_3)_3$ and $NaYI_4O_{12}$ are 23 and 11 pm V^{-1}, respectively. It should be noted that the differences in $\langle d_{eff}\rangle_{exp}$ are attributable to the phase-matching capabilities of the materials. In addition, using a model developed earlier and a $\beta(I^{5+}-O)$ of 140 × 10^{-40} m^4 V^{-1}, we were able to calculate $\langle d_{eff}\rangle_{calc}$ for each compound. In doing so, we obtained 15 and 25 pm V^{-1} for $La(IO_3)_3$ and $NaYI_4O_{12}$, respectively.

Piezoelectric Measurements. Converse piezoelectric measurements were performed on $La(IO_3)_3$ and $NaYI_4O_{12}$. Briefly, with the converse piezoelectric measurement, a voltage is applied to the sample that produces a macroscopic deformation.[2] A maximum voltage of 700 V was applied to both samples. Exceeding this voltage causes irreversible damage to the sample. With each sample, 20 measurements were performed and an average was taken. Graphs of the piezoelectric data have been deposited as Supporting Information. The piezoelectric charge constant, d_{33}, was calculated from

$$\Delta L = SL_0 \sim Ed_{33}L_0$$

where ΔL is the displacement of the sample, L_0 is the sample thickness (m), S is the strain ($\Delta L/L_0$), and E is the electric field strength (V m^{-1}). We estimate d_{33} values of 5 and 138 pm V^{-1} for $La(IO_3)_3$ and $NaYI_4O_{12}$, respectively. These values are consistent with other iodates such as $LiIO_3$ (d_{33} = 92 pm V^{-1}), KIO_3 (d_{33} = 39 pm V^{-1}), and $3La(IO_3)\cdot HIO_3\cdot 7H_2O$ (d_{33} = 19 pm V^{-1}).[37−39]

Structure−Property Relationships. To better understand structure−property relationships as well as the asymmetric coordination environment of I^{5+}, we calculated the local dipole moment for all of the reported iodates. This approach has been described earlier with respect to metal oxyfluoride octahedra.[40,41] We recently reported the dipole moments for $Te^{4+}O_3$ and $Te^{4+}O_4$ polyhedra.[42] We found that the average

Table 4. Calculation of Dipole Moments for IO_3, IO_4, and IO_5 Polyhedra

compound	species	dipole moment (D)
β-$Cs_2I_4O_{11}$	$I(1)O_4$	11.6
	$I(2)O_4$	12.9
	$I(3)O_4$	13.2
	$I(4)O_3$	13.3
$Rb_2I_6O_{15}(OH)_2\cdot H_2O$	$I(1)O_4$	12.5
	$I(2)O_4$	13.8
	$I(3)O_4$	10.0
	$I(4)O_3$	14.4
	$I(5)O_3$	13.7
	$I(6)O_3$	13.8
$La(IO_3)_3$	$I(1)O_3$	12.7
	$I(2)O_3$	15.1
	$I(3)O_3$	14.2
	$I(4)O_3$	15.3
	$I(5)O_3$	13.8
	$I(6)O_3$	13.2
	$I(7)O_3$	14.4
	$I(8)O_3$	14.9
	$I(9)O_3$	13.6
$NaYI_4O_{12}$	$I(1)O_4$	13.7
	$I(2)O_4$	14.2
	$I(3)O_3$	13.6
	$I(4)O_3$	13.3
	$I(5)O_3$	13.8
	$I(6)O_3$	12.9
	$I(7)O_3$	13.9
	$I(8)O_3$	14.2
α-$Cs_2I_4O_{11}$[30]	$I(1)O_5$	7.0
	$I(2)O_3$	9.0
$D(I_3O_8)$[43]	IO_3 × 2 (average)	12.2
	IO_4	9.5
$H(IO_3)(I_2O_5)$[44]	IO_3 × 2 (average)	12.0
	IO_4	10.4
$Ba(MoO_2)_6(IO_4)_2O_4(H_2O)$[45]	IO_4	11.1
I_2O_5[46]	IO_4 × 2 (average)	9.5
IOF_3[47]	IOF_3	11.3
KIO_2F_2[48]	IO_2F_2	9.3
$(IOF_2)(IO_2F_4)$[49]	IO_3F_2	6.0
$(NO)(HF_2)(IF_5)$[50]	IF_5	10.2
$(NO)(NO_3)(IF_5)$[51]	IF_5	12.0
$CsIOF_4$[52]	IOF_4	6.9
IO_3 polyhedra	IO_3 (average)	13.4
24 examples[a]	(range)	9.0−15.3
IX_4 polyhedra	IX_4 (average)	11.5
15 examples[a]	(range)	8.8−14.2
IO_5 polyhedra	IX_5 (average)	8.4
5 examples[a]	(range)	6.0−12.0

[a] In the Supporting Information

(36) Goodey, J.; Broussard, J.; Halasyamani, P. S. *Chem. Mater.* **2002**, *14*, 3174.
(37) Hamid, S. A. *Phys. Status Solidi A* **1977**, *43*, K29.
(38) Abrahams, S. C.; Bernstein, J. L. *J. Chem. Phys.* **1978**, *69*, 2505.
(39) Landolt, H., Ed. *Numerical Values and Functions from the Natural Sciences and Technology (New Series)*; Group 3: Crystal and Solid State Physics; Springer-Verlag: Berlin, 1979; Vol. 11.
(40) Maggard, P. A.; Nault, T. S.; Stern, C. L.; Poeppelmeier, K. R. *J. Solid State Chem.* **2003**, *175*, 25.
(41) Izumi, H. K.; Kirsch, J. E.; Stern, C. L.; Poeppelmeier, K. R. *Inorg. Chem.* **2005**, *44*, 884.
(42) Ok, K. M.; Halasyamani, P. S. *Inorg. Chem.* **2005**, *44*, 3919.
(43) Stahl, K.; Svensson, C.; Szafranski, M. *J. Solid State Chem.* **1993**, *102*, 408.
(44) Feikema, Y. D.; Vos, A. *Acta Crystallogr.* **1966**, *20*, 769.
(45) Sykora, R. E.; Wells, D. M.; Albrecht-Schmitt, T. E. *Inorg. Chem.* **2002**, *41*, 2697.
(46) Fjellvag, H.; Kjekshus, A. *Acta Chem. Scand.* **1994**, *48*, 815.
(47) Edwards, A. J.; Taylor, P. *J. Fluorine Chem.* **1974**, *4*, 173.
(48) Abrahams, S. C.; Bernstein, J. L. *J. Chem. Phys.* **1976**, *64*, 3254.
(49) Gillespie, R. J.; Krasznai, J. P.; Slim, D. R. *J. Chem. Soc., Dalton Trans.* **1980**, 481.
(50) Mahjoub, A. R.; Leopold, D.; Seppelt, K. *Eur. J. Solid State Inorg. Chem.* **1992**, *29*, 635.
(51) Zhang, X.; Seppelt, K. *Z. Anorg. Allg. Chem.* **1998**, *624*, 667.
(52) Ryan, R. R.; Asprey, L. B. *Acta Crystallogr., Sect. B* **1972**, *28*, 979.

local dipole moment for TeO_3 and TeO_4 polyhedra are similar, 8.6 and 8.7 D (D = debye), respectively. With the iodate polyhedra, the lone pair is given a charge of −2 and is localized 1.23 Å from the I^{5+} cation. This I^{5+}−lone pair distance is based on earlier work by Galy and Meunier.[4] For comparison, we have also calculated the local dipole moment for other iodates (see Table 4). In fact, an examination of 24 examples of IO_3, 15 of IX_4 (X = O or F), and 5 of IX_5 polyhedra resulted in average dipole moments of 13.4, 11.5, and 8.4 D, respectively. With this local dipole moment information, we can estimate the total dipole moment for each structure. In doing so, we obtain 7.7 D (0.0032 esu cm $Å^{-3}$) and 49.5 D (0.0208 esu cm $Å^{-3}$) for $La(IO_3)_3$ and $NaYI_4O_{12}$, respectively. The substantially larger dipole moment in $NaYI_4O_{12}$ compared with $La(IO_3)_3$ can be attributed to a greater amount of "constructive addition" of the iodate moments. The result of this larger moment is consistent with the measured d_{33} values; i.e., $d_{33}(NaYI_4O_{12})$ = 138 pm V^{-1}, whereas $d_{33}(La(IO_3)_3)$ = 5 pm V^{-1}. Interestingly, the SHG efficiencies are identical, 400 × α-SiO_2, for both materials. This indicates that other factors, in addition to the constructive addition of dipole moments, are responsible for the SHG efficiency.

Acknowledgment. We thank the Robert A. Welch Foundation for support. This work was also supported by the NSF-Career Program through Grant DMR-0092054. P.S.H. is a Beckman Young Investigator. We also acknowledge Yushin Park and Prof. Rigoberto Advincula for assistance in obtaining the Raman spectra.

Supporting Information Available: X-ray crystallographic files for β-$Cs_2I_4O_{11}$, $Rb_2I_6O_{15}(OH)_2 \cdot H_2O$, $La(IO_3)_3$, and $NaYI_4O_{12}$ in CIF format, calculated and observed X-ray diffraction patterns, TGA diagrams for all of the compounds, phase-matching curves, displacement versus electric field loops for $La(IO_3)_3$ and $NaYI_4O_{12}$, IR and Raman spectra, and dipole moment calculations. This material is available free of charge via the Internet at http://pubs.acs.org.

IC051340U